This article has been accepted for publication in IEEE Sensors Journal. This is the author's version which has not been fully edited and content may change prior to final publication. Citation information: DOI 10.1109/JSEN.2024.3487757

A Novel Self-Powered Wireless Rollers Rotational Speed Monitoring System

Shiheng Zhou, Tingcong Ye*, Lei Liu, Zhengmin Zhang, Michael Hayes, Ningning Wang*, Member, IEEE

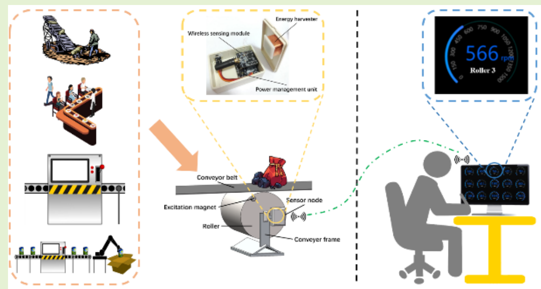

***Abstract*—In this paper, a novel energy harvesting—based, self-powered wireless speed monitoring system has been developed for monitoring the rotational speed of rollers without any modifications to existing rollers and conveyor systems. This innovative solution comprises multiple wireless sensor nodes, a Zigbee coordinator, a 4G module, and an Ali Cloud Computing based visualization interface. Each compact wireless sensor node, housed within a 68mm×52mm×25mm plastic box. It is equipped with an energy harvester, a power management unit, and a wireless sensing module. The energy harvester converts the rollers' kinetic energy into electrical energy. A comprehensive transient model has been developed to precisely predict the harvester's performance. The power management unit ensures reliable rectification, storage, and regulation of the electrical power generated. The optimized energy harvester achieves an output power of 23.5 mW at 800 rpm and 1.8 mW at 100 rpm. Under laboratory conditions, the energy harvester can charge a 0.1F supercapacitor to 5V in 85 seconds at 600 rpm, corresponding to a power level of 14.7mW. The wireless sensing module collects speed information from rollers and transmits it to a base station connected to the cloud via a 4G telecommunication network. Ultimately, the real-time rotational speeds of all rollers are visualized using a custom-designed user interface. Finally, the effectiveness of the self-powered wireless roller speed monitoring system is successfully demonstrated in a test bed.**

***Index Terms*—Electromagnetic, Energy harvester, Self-powered, Power Management, Wireless Sensor Networks.**

I. Introduction

To date, various belt conveyors are widely used to transport a wide variety of bulk materials over varying distances in large industries, particularly in mining and ports. As critical industrial equipment, belt conveyors are prone to several common failures, such as wear and tear of belt, faulty rollers, and malfunctioning motors. All these failures not only lead to unexpected plant shutdowns and significant production losses but also pose serious risks to personnel safety. Over time, various approaches have been developed and applied to detect faulty components and to provide preventive maintenance. The most commonly adopted approaches are to inspect the belt [1] and drive units including motors [2], [3] and gearboxes [4]. However, a belt conveyor system also includes a substantial number of rollers [5] which are essential parts designed to support the belt and minimize movement resistance. A faulty roller typically exhibits a rotational speed slower than standard or becomes completely immobilized. When just one roller fails, there is a risk of sharp broken parts cutting the belt [6] or surface abrasion leading to catastrophic fires and potential loss of life [7]. In order to monitor the health of rollers and conveyors during operation, several condition monitoring systems are currently in use, employing techniques like neural networks [8], [9], [10]. However, these monitoring systems primarily rely on measuring the vibration of bearings or analyzing acoustic signals, which are easily influenced by environmental factors. A variety of intelligent belt conveyor inspection systems also have been proposed [11] [12], designed to monitor the condition of rollers. However, these systems, whether hand-held or wired, are still far from ideal. They either lack the capability to provide continuous real-time monitoring on-site or are difficult to deploy due to the considerable effort required for cabling and maintenance.

Rollers are typically spatially distributed in massive quantities over a long distance in the mining industries, which makes it even more challenging in developing an effective intelligent monitoring system for their condition. Although unmanned drones have been proposed as a means to inspect belt conveyors over a long distance [13], their effectiveness in detecting faulty rollers has yet to be proven. Moreover, there is currently no viable solution for real-time detection of roller rotational speeds. An ideal intelligent roller rotational speed monitoring system would be wireless to eliminate the costs

Manuscript was submitted on XXXX, 2024. This work was supported in part by the Zhejiang Provincial Natural Science Foundation under Grant LD21F040001, and in part by the Micropower Solutions Co., Ltd.
Corresponding authors: Ningning Wang, ning.wang@hdu.edu.cn; Tincong Ye, tingcong.ye@hdu.edu.cn.

S.H. Zhou, T.C. Ye, L. Liu, Z.M. Zhang, N. Wang are with School of Electronics and Information Engineering, Hangzhou Dianzi University, Hangzhou, 310018, China (e-mail: zhoushiheng@hdu.edu.cn; tingcong.ye@hdu.edu.cn; dzlliu@hdu.edu.cn; zhangzhengmin@hdu.edu.cn; ning.wang@hdu.edu.cn). M. Hayes is with Tyndall National Institute, University College Cork, Cork, T12 R5CP, Co. Cork, Ireland (e-mail: michael.hayes@tyndall.ie).

associated with cabling and would need to be energy-autonomous to avoid the expense of battery maintenance. This work aims to develop a self-powered wireless sensor network (WSN) for monitoring the rotational speed of rollers in a conveyor system.

II. Energy Harvesting and WSNs

Wireless Sensor Networks (WSNs) have demonstrated significant benefits for specific applications in harsh environments, particularly for distributed condition monitoring tasks [14]. WSN nodes are generally powered by onboard batteries, which require periodic replacement due to their limited energy capacity [15]. In most cases, this necessity for regular maintenance incurs considerable costs and logistics overhead, hindering the widespread adoption of WSNs in practical applications. Given this limitation, exploring alternative power sources to either replace or supplement the battery becomes highly desirable [16].

In the context of rollers, kinetic energy is inherently available due to the rollers' rotation through friction with conveyor belts [17]. To date, many rotational energy harvesters have been developed utilizing piezoelectric conversion techniques [18], [19]. These demonstrated piezoelectric energy harvesters consist of either cantilever or buckling beams with bimorph or unimorph structures [20]. However, piezoelectric beams for rotational energy harvesting are most efficient only when the vibration excitation frequency closely matches the resonant frequency of the structure [21]. For a belt conveyor, the rotation speed of rollers can vary widely due to the belt operating at different speeds depending on the system configuration and work load. Therefore, the proposed piezoelectric energy harvester may not be suitable for powering sensor nodes integrated into the rollers, which could rotate at varying speeds.

Electromagnetic conversion is another way of harvesting rotational energy, typically employing permanent magnets and coils [22], [23], [24]. Miao G et al. proposed a low-frequency rotational electromagnetic energy harvester using a magnetic plucking mechanism [25]. Using the novel structure to pluck a cylindroid generating magnet during each rotation, the resetting effect provides a new way to stabilize the output voltage and enhances the energy harvesting performance. Dai Xiaoyi et al. designed a hybrid energy harvesting system tailored for self-powered applications in shared bicycles [26]. The power generation module within the system utilizes a magnet array on the spokes to cut magnetic lines and deforms a piezoelectric sheet to harvest the kinetic energy of the wheel. Jiahong Lin et al. used a stationary coil array and a rotating magnetic rotor structure to collect kinetic energy from human motion. At a running speed of 8 km/h, the maximum voltage and average power density can reach to 1.92 V and 0.2 mW/cm^3, respectively[27]. M. A. Halim et al. made a structure that uses rotating eccentric mass to collect electromagnetic energy [28]. The prototype generates an average power of 55 µW at ±25 degrees rotational amplitude. There are other electromagnetic energy harvesting designs reported, such as a weighted-pendulum-type electromagnetic generator [29], and a rotational electromagnetic energy harvester driven by a twist-driving system [30]. From both a technical and practical standpoint, electromagnetic energy harvesters are well-suited for converting rotational energy into electrical energy due to their simplicity, ease of fabrication, and environmental friendliness. However, most of the aforementioned electromagnetic energy harvesters are not suitable for collecting kinetic energy from rollers because they require either the coil or the magnet to rotate alongside with the rollers. This necessity would entail significant modifications to the rollers themselves. It seems to be an effective approach to pluck a cylindroid generating magnet by attaching an excitation magnet to a rotational object. This is an effective approach to harvest the kinetic energy at frequencies ranging from 1 to 3.5Hz, which corresponds to rotational speeds of 60 to 210rpm[25]. Nevertheless, the reported approach is inadequate for roller speed monitoring in a convey systems where the typical rotational speed is 300rpm or higher. Moreover, a significant challenge still remains in extracting sufficient power levels within the confined spaces available in many applications.

In this paper, we present a novel energy harvesting based, self-powered wireless speed monitoring system designed to monitor the rollers' condition in belt conveyors. The system comprises an electromagnetic energy harvester and a power management unit, which together convert the rollers' kinetic energy into electrical energy to power the WSN modules for monitoring rotational speed. Each node transmits real-time speed information of its corresponding roller to a base station, which is connected to the cloud through a 4G telecommunications network. The real-time rotational speeds of all monitored rollers are displayed using a custom-designed user interface. The self-powered roller's wireless rotational speed monitoring system is finally successfully demonstrated in a test bed. The remainder of this paper is organized as follows: Section III introduces the framework of the self-powered wireless roller speed monitoring system and outlines its main functions. Section IV describes the design and theoretical model of the proposed magnetically actuated electromagnetic rotational energy harvester. Section V investigates the power management circuit and the power consumption of the wireless sensor node across different operational modes. The effectiveness of the proposed energy harvester, the power management unit, and the entire wireless rotation speed monitoring system is demonstrated in Section VI. Conclusions are provided in Section VII.

III. System Configuration

The self-powered real-time wireless rotation speed monitoring system developed in this work is designed for monitoring the operational conditions of rollers in a conveyor. The system configuration is shown in Fig. 1, which comprises multiple wireless sensor nodes, a Zigbee coordinator, a 4G module, and an Ali Cloud Computing-based visualization interface. Compared with other communication means, ZigBee is a widely adopted communication method that offers a balance between low power consumption and a reasonable transmission range. In coal mines, 4G is a widely adopted and commonly used long range telecommunication infrastructure. Each Zigbee sensor node captures the rotational speed of the roller that it is monitoring, and transmits this data to the Zigbee coordinator. The Zigbee coordinator then uploads the data to the Ali Cloud through the 4G module. Given that there is one

This article has been accepted for publication in IEEE Sensors Journal. This is the author's version which has not been fully edited and
content may change prior to final publication. Citation information: DOI 10.1109/JSEN.2024.3487757

sensor node per roller, there would be dozens of sensor nodes and a single coordinator installed for each conveyor section. The data packets are tagged with a unique serial number to identify the sending node. Ultimately, the data is processed and displayed in real time through a user-friendly interface on either computers or smartphones.

To achieve a cable-free and maintenance-free system, the key challenge lies in making all wireless sensor nodes self-sustaining. To enable energy autonomous for each sensor node, an energy harvester along with a power management unit has been developed and integrated in each sensor node box. Consequently, every wireless sensor node in the system consists of an energy harvester, a power management unit, and a wireless sensing module, all housed in a compact plastic box, as shown in Fig. 2. The wireless sensing module is mounted atop the power management unit to optimize space. A Hall sensor is affixed to the internal wall of the sensor node's casing to measure the external magnetic field.

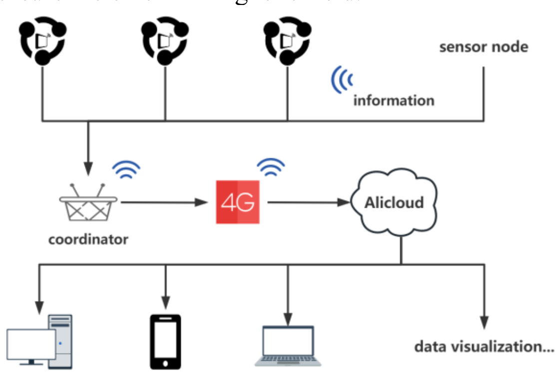

Fig. 1. Diagram of a self-powered roller speed monitoring system.

The sensor node box is installed on the conveyer's support frame, near the side of the rotating roller, as shown in Fig. 3. An excitation magnet (EM) is attached to the side of the roller with its north or south pole oriented towards the sensor node. As the roller rotates, the EM passes the senor node once per revolution. The magnetic field produced by the excitation magnet will force the ring-shaped generator magnet (GM) housed within the energy harvester to rotate, thereby transferring the rollers' rotational kinetic energy to the ring magnet. The kinetic energy of the GM is converted into electrical energy by the energy harvester through the fluctuating flux within the coil. The generated electrical energy is further rectified, stored, and regulated to a stable DC voltage by the power management unit. The wireless sensing module comprises a microprocessor unit (MCU), a Zigbee wireless module, and a Hall sensor. The MCU reads the Hall sensor's status, and the collected data is transmitted from the Zigbee node to the Zigbee coordinator. The design and development of the energy harvester and its associated power management unit are described in the following section.

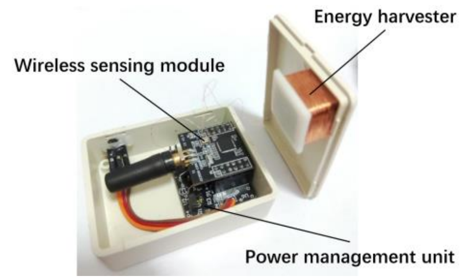

Fig. 2. A sensor node box containing an energy harvester, a power management unit and a WSN module.

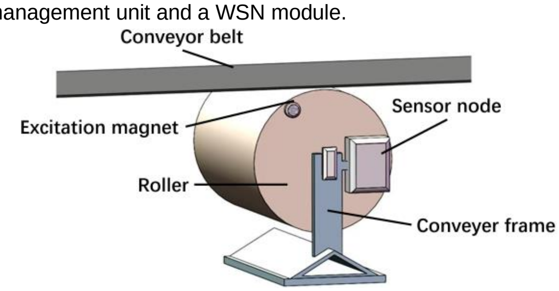

Fig. 3. A 3D drawing of a sensor node installed on the frame of a conveyor to monitor the rotational speed of a roller.

IV. System Design and Modelling

A. Energy Harvester Design and Modelling

There is an energy harvester housed within each sensor node box. Each energy harvester consists of a casing, a rotating shaft, a ring-shaped NdFeB GM, two bearings, and a copper coil wound around the casing. Fig. 4(a) illustrates an assembled energy harvester with an external orbiting EM. The energy harvester is securely mounted within the sensor node box, while the EM is attached to the roller that orbits as the roller rotates. An exploded view of the energy harvester is shown in Fig. 4(b). As opposed to the re-setting mechanism using an additional magnet, this energy harvester uses a free-wheeling mechanism to enhance the rotating speed of GM, thus to improve the power output. The two bearings are embedded in the top and bottom covers to reduce the friction. A shaft passes through the GM and is fixed to the bearings. Two hoops are used to not only hold the casing parts together, but also act as a mold for winding the copper coil. The copper coil is wrapped around the casing. It is held in place by these two hoops. Excluding the two hoops, the casing measures 14.5mm×14.5mm×14mm, with an inner space of 13mm×13mm×9mm. The shaft is designed to be 11mm long and 3mm in diameter. 3D printing was used to manufacture the casing parts and hoops. Photosensitive resin was chosen as the printing material due to its low viscosity, minimal curing shrinkage, rapid curing rate, and high degree of curing.

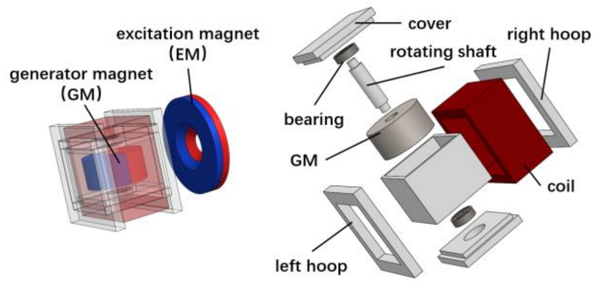

Fig. 4. Energy harvester module (a) Side view and a GM with an external orbiting EM; (b) Exploded view of the proposed energy harvester module.

The dimensions of the GM have been specifically chosen: an outer diameter of 12mm, and inner diameter of 3mm, and a height of 6mm. Copper wire with a 0.08mm diameter is used for the coil. The number of turns of the coil is 1562 turns for the original prototype.

The radially magnetized GM within the energy harvester is actuated by the EM attached to the side of the monitored roller. For ease of installation, a ring-shaped NdFeB magnet with a recessed hole was selected as the EM. As the roller rotates, the EM passes by the sensor node box once per revolution, causing the GM within the energy harvester's casing to rotate. The rotation of the GM leads to alternating magnetic flux within the coil, which in turn induces an AC voltage.

The induced voltage, V, can be expressed as:

$$V = N\frac{d\emptyset}{dt} \tag{1}$$

where N is the number of turns of the coil, Φ is the magnetic flux inside a single-turn coil, t is the time.

Due to the intricate distribution of the flux within the harvester, the flux linkage of the coil was obtained using finite element simulation in this work. Fig. 5 illustrates the positioning and angular relationships between the GM and the coil. The GM is centered within the coil. The angle between the north pole of the GM and the central axis of the coil is θ. The variation of the flux linkage as a function of the angle θ is shown in Fig. 6. When the angle θ is zero or π rad, the magnetic flux through the coil attains its maximum absolute value. When the angle θ is $\pi/2$ or $3\pi/2$ rad, the flux linkage of the coil is 0 Wb. It can be seen from the curve that the flux linkage reaches its maximum absolute value of 0.055 Wb at point M1 and point M3, and it decreases to 0 Wb at point M2. The finite element simulation results indicate that the maximum flux linkage generated by the excitation magnet is 0.006Wb at the point where it is closest to the coil. In contrast, the flux linkage generated by the generator magnet (GM) is approximately 0.6Wb, which is two orders of magnitude greater than that produced by the EM. Therefore, the voltage generated by the passing EM itself is negligible.

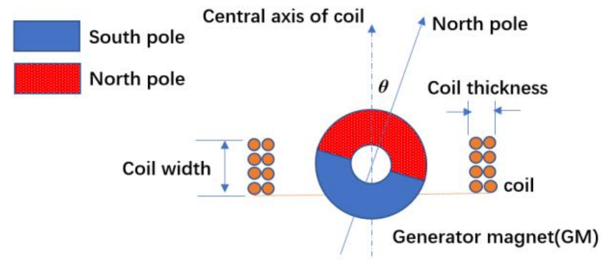

Fig. 5. Generator magnet (GM) and coil within the energy harvester.

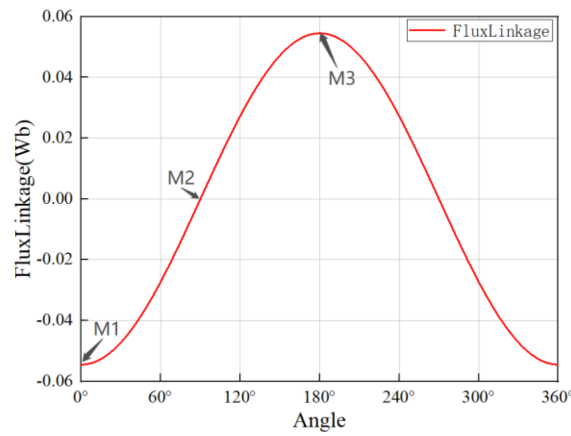

Fig. 6. Magnetic flux linkage simulated using finite element simulation.

Using the curve fitting technique, the flux linkage curve shown in Fig. 6 can be expressed as:

$$\emptyset(t) = a_0 + a_1\cos(\omega t) + b_1\sin(\omega t) \tag{2}$$

where a_0, a_1 and a_2 are curve fitting parameters, and ω is the angular velocity of the GM.

For Equation (2) to match the curve shown in Fig. 6, the values for a_0, a_1 and a_2 are -0.0000007849, -0.05454, and -0.00004062, respectively.

Substituting (2) into (1), the output voltage can be expressed as:

$$U(t) = \frac{d\emptyset(t)}{dt} = -a_1\omega\sin(\omega t) + b_1\,\omega\cos(\omega t) \tag{3}$$

Hence, for any given position of the GM, the induced voltage can be obtained if the instant angular velocity is known.

The instant angular velocity, ω, of the GM can be expressed as:

$$\omega(t) = \omega_0 - at \tag{4}$$

where ω_0 is the initial angular velocity of the GM, a is the angular acceleration of the GM, t is the time elapsed.

The instant angular acceleration a of the GM can be calculated by:

$$a = \frac{F_m + F_f + F_e}{I_r} \tag{5}$$

where F_m is the torque caused by the external EM, F_f is the mechanical damping torque caused by the friction, and F_e is the electromagnetic damping torque due to the induced load current, and I_r is the rotational inertia.

The mechanical damping torque, caused by friction, can be calculated using the recorded open circuit output voltage waveform of the harvester after imparting an initial angular velocity to the GM. A typical decaying open-circuit output voltage of the coil, measured by an oscilloscope following the passage of the external EM past the GM, is shown in Fig. 7. At the beginning, as the excitation magnet (EM) approaches the generator magnet (GM), the GM will first quickly start to rotate and align itself with the magnetic field generated by the EM. Due to the attractive force between the two magnets and the rotational inertia, the GM will oscillate slightly back and forth, resulting in an initial small voltage output. When the EM starts to rapidly depart from the GM, it is at this point that the EM truly transfers its kinetic energy to the GM via the magnetic force. This results in the high-speed rotation of the GM, and hence the generation of high voltage peaks. Because of the mechanical damping torque, the angular velocity of the EM gradually diminishes until it reaches zero. So does the induced voltage. At point D1 and D2, the induced voltages are 19V and 6V, respectively. Applying Equation (3), the angular velocities at point D1 and point D2 are calculated to be 110.9π rad/s and 35π rad/s, respectively. Given that the time interval between D1 and D2 is 0.26s, the damping torque F_f can be derived as follows:

$$F_f = I_r \frac{(\omega_2 - \omega_1)}{\Delta t} \tag{6}$$

where ω_1 is the angular velocity at D1, ω_2 is the angular velocity at D2, Δt is the time interval between the two points.

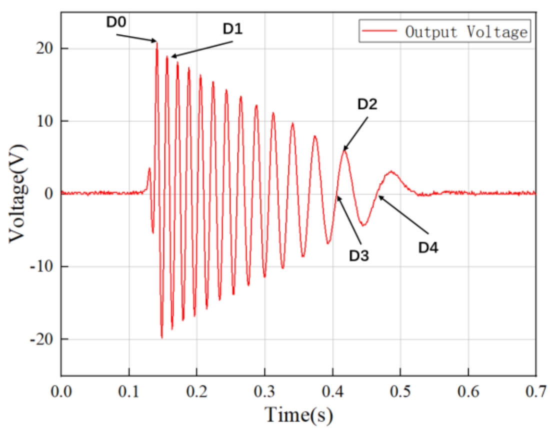

Fig. 7. A typical output voltage waveform measured from the energy harvester under no load condition.

The rotational inertia of the GM regarding its central axis can be calculated by:

$$I_r = \frac{1}{2} M (R_1^2 + R_2^2) \tag{7}$$

where R_1 is the inner radius of the GM, R_2 is the outer radius of the GM, and M is the mass of the GM. The mass of the GM used in this design is 477g. Its rotational inertia is calculated to be 9.125×10^{-8} kgm^2.

Once the rotational inertia is known, the mechanical damping torque as well as the angular acceleration can be obtained. The calculated mechanical damping torque is 8.37×10^{-5} N·m, and the angular acceleration is 292π rad/s^2.

The waveform shown in Fig. 7 is the output voltage at no load condition. Both F_m and F_e are zero, and there are no external forces except for friction. The angular acceleration a is a constant value. The instant angle, θ, of the GM can be expressed as:

$$\theta(t) = \omega_0 t + \frac{1}{2} a t^2 \tag{8}$$

The initial angular velocity of the GM, ω_0, can be determined using the peak voltage value at point D0 and Equation (3), yielding a value of 122.6π rad/s. With both the initial angular velocity and the angular acceleration known, the angle of the GM and its instantaneous angular velocity can be calculated using Equation (4) and (6), respectively. These calculations, in turn, gives the instantaneous induced voltage value using Equation (3). Both the simulated and measured voltage waveforms are shown in Fig. 8. As evident from the figure, the simulated voltage waveform matches well with the measured one. This confirms the accuracy of the modelling approach for the rotational inertia and mechanical damping of the GM.

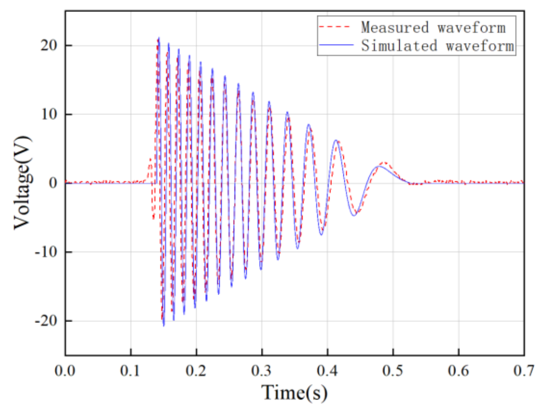

Fig. 8. Comparison of the measured and simulated output voltage waveforms under no-load condition.

When the coil is connected to a load, it forms a current loop that subsequently generates a magnetic field. This field interacts with the magnetic field produced by the permanent magnet GM already present in the energy harvester. According to the energy conservation theorem, the work done by the electromagnetic damping torque, F_e, is eventually converted into electrical output. F_e can be calculated by:

$$F_e \omega = \frac{V^2}{R_t} \tag{9}$$

where the right-hand part of the equation is the generated electric power of the harvester, V is the induced voltage, R_t is the total resistance in the current loop, and ω is the instant angular velocity of the GM.

The rotation of the GM within the energy harvester is triggered by the magnetic force between the EM and the GM. The motion of the GM is determined by its initial motion as well as the magnetic force exerted by the passing EM. To accurately predict the motion of the GM and evaluate the potential electrical power output, it is essential to precisely model the magnetic force between the GM and the orbiting EM.

As shown in Fig. 9, a 3D simplified model was used to simulate the magnetic field surrounding the GM as the EM moves in a straight line from left to right. The torque exerted on the GM is determined by the distance between the GM and the EM and the angle orientation of their respective north poles.

The minimum distance between the EM and the GM is 20mm in this simulation.

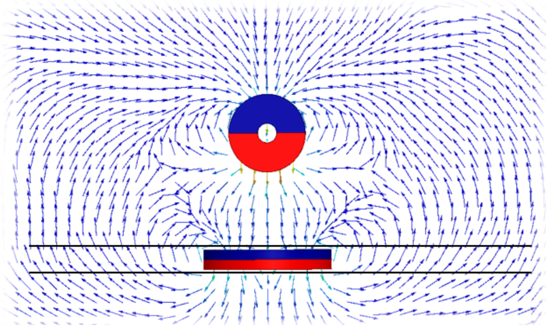

Fig. 9. A simplified 3D model showing the simulated magnetic field between the two magnets.

The angle of the GM is defined as 0 rad when its north pole is perpendicular to the movement trajectory of the external EM. In the model shown in Fig. 10, the origin of the coordinate system is defined as the position where the EM is directly facing the GM, at which point the magnetic torque F_m on the GM is 0 as expected. The simulated magnetic torque on the GM at a 0 rad rotation angle, as the position of the EM varies from -70mm to 70mm, is shown in Fig. 10. The simulation reveals that the magnetic torque decreases rapidly once the distance exceeds 70mm. A curve fitting technique was used to derive a closed-form equation for the magnetic torque at the 0 rad angle, as shown below:

$$F_m = a_1 \sin(\omega x) + a_2 \sin(2\omega x) + a_3 \sin(3\omega x) + a_4 \sin(4\omega x) + a_5 sin(5\omega x) + a_6 sin(6\omega x) \quad (10)$$

where a_1 = 1.607, a_2 = 1.557, a_3 = 1.053, a_4 = 0.5281, a_5 = 0.2436, a_6 = 0.06942, ω = 0.0419.

As shown in Fig. 10, the fitted curve aligns closely with the simulation results. The same approach was applied to generate a series of magnetic torque curves for the GM at various angles, with the position of the EM varying from -70mm to 70mm. In the finite element simulations for the series of magnetic torque curves, the angles are varied from 0 to $2\boldsymbol{\pi}$ in increments of $\boldsymbol{\pi}/36$ rad.

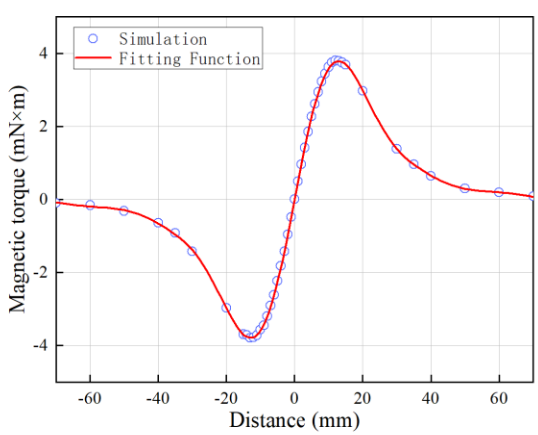

Fig. 10. Simulated magnetic torque on the GM and the fitted curve at 0 rad angle with different distance.

By incorporating the relevant equations into a Simulink-based program, a transient analytical model for the energy harvester is now in place. This model enables us to calculate the instantaneous angular velocity of the GM at any given time, regardless of its initial position and orientation. As a result, we can predict the output voltage waveforms of the energy harvester across different roller speeds, both under loaded and unloaded conditions.

The induced AC voltage needs a rectification circuit so to charge an energy storage element. The charging process can be expressed as:

$$U = U_0 + (U_f - U_0)(1 - e^{\frac{-t}{RC}}) \quad (11)$$

where U is the resulting voltage of the energy storage element, U_0 is the initial voltage, U_f is the voltage of the voltage source, R is the equivalent resistance of the charging circuit, C is the capacitance value, and t is the charging time.

The energy stored inside the energy storage element Q can be calculated by:

$$Q = \frac{1}{2} C U^2 \quad (12)$$

where C is the capacitance value of the energy storage element.

By knowing the energy Q of the energy storage element and charging time, the available power of the energy harvester under different conditions can be estimated. It is important for the subsequent design of power management circuits, control methodology of embedded devices, and system power consumption analysis.

B. Coil Design

To maximize output power for applications that require more frequent sensing and data transmission tasks, it is critical to optimize the energy harvester. Several factors were taken into consideration during the development, including the availability of materials, cost, ease of assembly, and the size of the sensor node. The wireless module, sensor node casing, permanent magnets, and bearings are all off-the-shelf components used in this development. There are limited sizes of magnets available on the market. The chosen size should be not too small, considering the power generation and ease of handling, and not too large, considering the space constraints. Given the fixed dimensions the GM and the energy harvester casing, the output power is influenced primarily by the coil parameters, such as wire diameter, coil width, and the number of turns, etc. Therefore, refining the coil design is essential to increase the power density of the harvester.

According to Equation (1), the induced voltage in the coil is directly proportional to the flux linkage, which is closely tied to the dimensions of the coil. The dimensions of the coil are mostly dictated by the size of the harvester casing. Among these dimensions, the coil's thickness, T_c, and width, W_c, are the only variables that can be adjusted during design, as shown in Fig. 5. This optimization aims to determine the optimal coil with and thickness to achieve maximum output power. The cross-sectional area of the coil, S, is defined as the product of T_c and W_c.

Finite element simulations were used to explore the relationship between flux linkage and coil width for different coil thicknesses can be obtained using, as depicted in Fig. 11(a). The simulation results indicate that, for a constant coil thickness, the flux linkage decreases as the coil width increases. Similarly, for a fixed coil width, the flux linkage decreases with an increase in coil thickness. This trend arises due to the higher magnetic flux density near the GM. A more spread-out coil, whether wider or thicker, results in a smaller average flux linkage per turn, reflecting the reduce concentration of magnetic flux.

In general, maximum output power occurs when the load resistance is matched to the coil resistance. The wire diameter and the number of turns do not influence the output power if the cross-sectional area of the coil remains constant. The results shown in Fig. 11. can be further applied to calculate the output voltage of the harvester with a matching load. The relationship between power and coil thickness with a fixed cross-sectional area of the coil is shown in Fig. 11(b). The ring magnet angular velocity is set at 33.33$\boldsymbol{\pi}$ rad/s in the calculation. Although a smaller cross-sectional area may seem advantageous for flux linkage, the output power actually increases with a larger area. This is because the output power is inversely proportional to the coil resistance while the resistance itself is inversely proportional to the cross-sectional area if the number of turns is fixed. Considering the generated power level and the size constraints of the coil, a wire diameter of 0.1mm was eventually chosen for constructing the final energy harvester prototype. The initial coil, which was 1mm thick with a wire diameter of 0.08mm, was replaced with a 2mm thick coil using 0.1mm wire. According to model predictions, the maximum output power of the prototype can be increased by 50.8% by this optimization.

After coil optimization, the performance of the original prototype and the final prototype was compared by testing their ability to charge an identical supercapacitor. It takes the optimized energy harvester prototype 85s to charge a 0.1F supercap to 5V, whereas it takes 150s for the original one under a rotational speed of 600rpm, which corresponds to a power level of 14.7mW. This represents a 43.3% reduction in charging time, indicating a significant improvement in the harvester's output power due to the optimized coil. The specifications of the final energy harvester prototype are detailed in TABLE I.

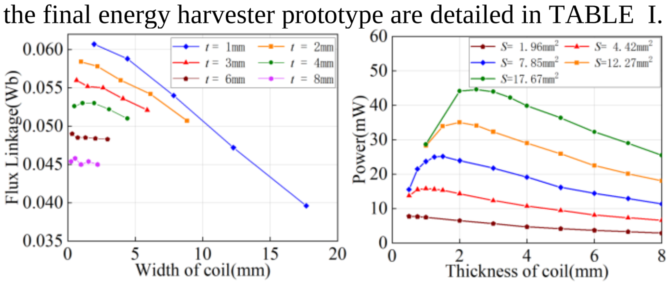

(a) (b)

Fig. 11. Simulation results using various coil width and thickness: (a) Maximum flux linkage at different coil widths; (b) Maximum power at different coil thicknesses (the GM's angular velocity is 33.33$\boldsymbol{\pi}$ rad/s).

TABLE I
PARAMETERS OF THE OPTIMIZED ENERGY HARVESTER PROTOTYPE

Parameters	Value
Casing of the energy harvester, mm	(L)14.5×(W)14.5×(H)14
Size of the hoops, mm	(L)20.5×(W)20×(H)2
Top and bottom covers, mm	(L)14.5×(W)14.5×(T)3
Length of the shaft, mm	11
Diameter of the shaft, mm	3
Diameter of the wire, mm	0.1
Turns of the coil, turns	1562
Resistance of the coil, Ohm	200
Inner diameter of the GM, mm	3
Outer diameter of the GM, mm	12
Thickness of the GM, mm	6
Inner diameter of the EM, mm	3
Outer diameter of the EM, mm	20
Thickness of the EM, mm	3

C. Power Management Unit Design

A power management unit has been developed in this work to condition the electrical energy harvested. A diagram of the power management unit is shown in Fig. 12, which includes a full bridge rectifier, an energy storage element, a voltage regulator, and a hysteresis control unit.

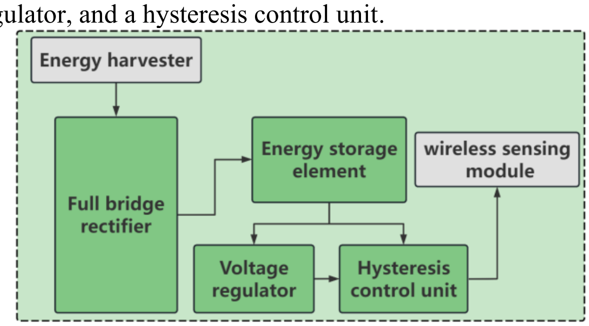

Fig. 12. Diagram of the power management unit.

The AC voltage generated by the energy harvester must first be rectified to charge the energy storage component. For this purpose, a full-bridge rectification using the ABS210 diode from ASEM is employed in this work due to its low leakage current of just 5uA and a short recovery time of 500ns.

Given that the subsequent WSN module requires a stable 3.3V supply, voltage regulation is achieved using the TPS79733 chip from Texas Instrument. This chip is selected for its ultra-low power consumption. It has an ultra-low quiescent current of only 1.2uA, which can greatly reduce the standby power consumption of the power management unit.

During the startup phase of the system, the wireless sensor network requires each Zigbee-based sensor node to connect to the Zigbee coordinator. Each connection attempt consumes approximately 65mJ of energy. If the initial attempt fails, subsequent retries will be made. If the energy storage element, i.e., a supercap in this case, starts powering the sensor node as soon as its voltage reaches 3.3V, its voltage will immediately drop below 3.3V due to the considerable amount of energy consumed by the connection attempts. The sensor node shuts down instantly once the voltage drops below 3.3V. The supercap needs time to recharge and reach 3.3V again. Hence, the system might never successfully start up due to repeated shutdowns. To prevent this "energy trap", a hysteresis switching circuit has been incorporated into the design between the energy storage element and the wireless sensing module. The hysteresis circuit is designed to power the wireless sensing module only when the supercap's voltage reaches 5V. The circuit automatically disconnects the wireless sensing module when the supercap's voltage falls below 3.6V. As a result, there is 602mJ of energy available in the 0.1F supercap for the initial connection attempt, ensuring the sensor node remains operational due to the low voltage protection. In this implementation, Texas Instruments' TLV521 milliwatt power op-amp chip is applied, which consumes only 350nA.

D. Wireless Sensing Module Design

The wireless sensing module developed in this work uses CC2530 chip as the core component of the Zigbee node. The CC2530 is a System on Chip (SoC) solution from Texas Instruments for IEEE 802.15.4, Zigbee and RF4CE applications. The sensor node is powered by the energy harvester and the power management unit. The CC2530 chip offers five operating modes including active, idle, PM1, PM2, and PM3.

In operation, the Zigbee sensor node needs to operate in active mode for a few seconds, measuring the speed and transmitting data. Subsequently, it enters a low-power sleep mode to minimize power consumption. At predetermined intervals, the node can wake up to resume its operations. If the node were to enter the lowest power consumption mode, i.e., PM3 sleep mode, it could only be awakened through a reset or an external I/O port interrupt, which would necessitate manual intervention. This does not align with the desired autonomous and maintenance-free nature of our target application. Alternatively, the PM2 sleep mode, while consuming slightly more power at 39uW, allows for wake-up via a pre-set timer. Therefore, the PM2 sleep mode was chosen for this design.

A Hall sensor is employed for rotational speed detection. Hall sensors are divided into different types, such as bipolar Hall, unipolar Hall, linear Hall, and omnipolar Hall. The sensor used in this work is an omnipolar Hall sensor from Huaxin. The EM passes the Hall sensor once for each revolution. Each revolution of the EM passes the Hall sensor once. The CC2530 chip detects a single positive square pulse from the Hall sensor per revolution. The accumulated pulse count over a defined interval is recorded, enabling the calculation of the average roller rotational speed through an algorithm.

V. Experiments and Model Verification

The energy harvester prototype has been constructed and tested to evaluate the harvester's model. The prototype test setup is shown in Fig. 13. A disc driven by an external motor was used to mimic a rotating roller. The EM was mounted on the outer surface of the disc. The disc's height was adjusted to ensure that the excitation magnet consistently passed the energy harvester at the same level as the EM's during each revolution. The distance between the excitation magnet and the energy harvester was set at 20 mm.

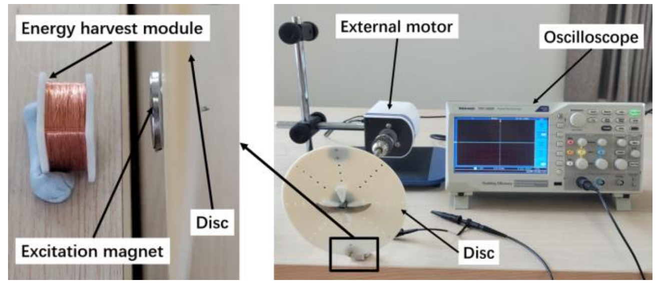

(a) (b)

Fig. 13. The experimental setup for the energy harvester.

The output voltage of the final energy harvester was measured by an oscilloscope when the rotation speed of the motor was set to 300 rpm. The measured voltages with and without a load are shown in Fig. 14(a) and Fig. 14(b), respectively. The output voltages with and without load predicted using the developed transient model are shown in Fig. 14(c) and Fig. 14(d), respectively. In both the test and the model calculations, the load resistance is equal to the coil's resistance. For the open circuit condition, the measured output voltage waveform of the harvester is unstable and uncertain owing to the random initial angle of the GM. This randomness was also observed in the results from the transient model. However, for the load condition, due to the electromagnetic damping, the speed of the GM decays much faster than that under open circuit condition. Hence, the induced voltage measured under load condition decays much faster than that under the open circuit condition. The results demonstrate that the transient model accurately predicts the energy harvester's output voltage under both load and unload conditions.

The model can be used to predict the Root Mean Square (RMS) output voltages of the energy harvester across any roller rotational speed. The predicted output RMS output voltages for the rotational speeds ranging from 0 rpm and 2000 rpm under load condition are shown inFig. 15. The tested voltages for speeds between 100 rpm and 800 rpm (limited by the drive motor's capability during testing) are also shown inFig. 15. The energy harvester generates an RMS output voltage of 2.17V at 800 rpm, and 0.603V at 100 rpm, respectively. At low operating speeds, the voltage waveform exhibits a highly irregular pattern, despite the relatively small RMS value. The induced voltage appears more akin to a series of pulses, with the instantaneous voltage level surpassing 5V. A standard full-bridge diode was used to rectifier the induced AC voltage. Given the coil resistance of 200Ω, these voltages correspond to an RMS output power of 23.5 mW at 800 rpm and 1.8 mW at 100 rpm. The results again confirm that the transient model can predict the output voltages with commendable accuracy. Notably, the induced RMS voltage is very low when the rotational speed drops below 100 rpm, primarily due to the low initial angular velocity of the GM triggered by the EM [20]. The re-setting mechanism proposed in [25] can be used to improve the power output when the speed is low. However, for the roller speeding monitoring in a convey system, the rotational speed is typically 300rpm or higher. The free-wheeling mechanism adopted in this work can considerably improve the output power. The induced RMS voltage increases with the rotational speed between 100 rpm and 1100 rpm because the roller's increasing rotational speed leads to an increased moving speed of EM, and hence the initial angular velocity of the GM. The induced voltage peaks at a certain rotational speed of EM, which is 1100 rpm in this case. The voltage becomes smaller once the EM's rotational speed exceeds 1100 rpm. This phenomenon is similar to that outlined in [20], which is due to the vibrational interference.

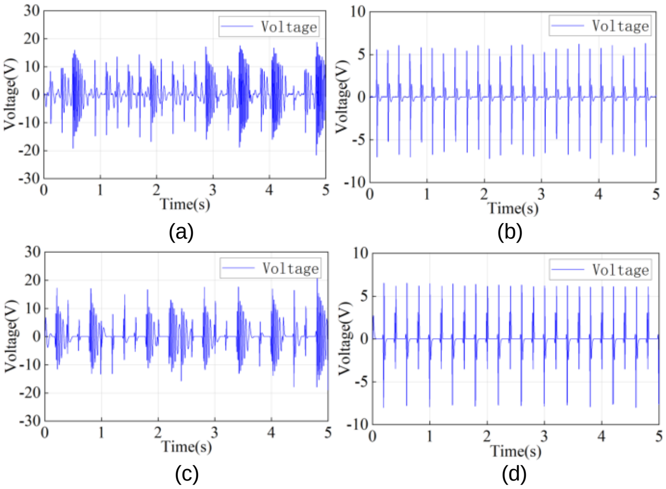

Fig. 14. Output voltage of the harvester (a) measured at 300rpm without load (b) measured at 300rpm with load (c) predicted at 300rpm without load (d) predicted at 300rpm with load.

TABLE II lists some recently reported rotational electromagnetic energy harvesters. In addition to the peak output power, the power density is also given in the table for a fair comparison. It can be seen from the table that the energy harvester developed in this work has relatively better performance than the other harvesters in terms of power and power density.

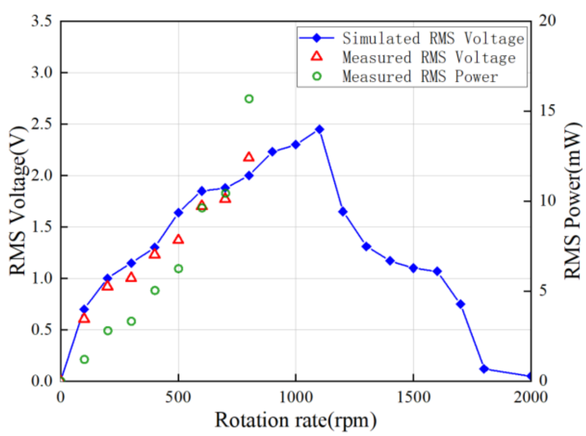

Fig. 15. Both measured and predicted RMS values of output voltage at different speeds and the measured RMS Power under load condition.

The power consumption characteristics of the WSN node also have been tested using KEYSIGHT's N6705C DC Power Analyzer. The test setup is shown in Fig. 16. The energy consumption of the Zigbee module can be precisely assessed under various operating modes using this setup. The power consumption measured on the sensor node under active mode is shown in Fig. 17(a). The node operates in active mode for approximately 1.8 seconds, with an average power consumption of 41 mW. The energy consumed for both data sensing and transmission is 73.8 mJ. After data sensing and transmission, the wireless sensor node enters sleep mode. In this mode, the measured current is 7.8uA, comprising 1uA for the wireless sensor node and 6.8uA for the power management module. The system power consumption of the node in sleep mode was only 39uW. The power consumption of the node for data transmission is shown in Fig. 17(b). Although the maximum power usage reaches 170 mW during this period, the data transmission process lasts only 7 ms and consumes 0.434 mJ of energy. Relative to the total energy consumed for the entire data sensing and transmission process, the energy consumption associated with data transmission is minimal. If the sensing interval is set to 30mins, the average power consumption of the node drops to 79.961uW, which is notably low compared to the power available from the energy harvester.

TABLE II
COMPARISON WITH OTHER ROTATIONAL ELECTROMAGNETIC ENERGY HARVESTERS

References	Volume (cm^3)	Frequency range (Hz)	Power (mW)	Power density ($mW\ cm^{-3}$)
Feng[23]	2	23.3-68.7[a]	0.0097[a]	0.00485
Miao[25]	11.25	1.5-4[b]	5.67	0.504
Lin[27]	32	0.67-2	6.4[c]	0.2
Halim[28]	8.48	0.67-1.25[d]	0.055	0.0065
This work	5.74	1.6-13.3[e]	23.5	4.1

[a]If the load resistance ranges from 100 to 400, the generated power is above 8 μW. The max. power is 9.7 μW, when the load resistance is 218Ω and the rotational speed is 3900 rpm (65Hz).
[b]The volume calculates the magnets, supports and baseplate with only the optimal θ and h2 at h1=20mm. The frequency is 1.5–4.0 Hz and the vehicle speed is 10.14–26.8 km/h.
[c]The energy harvester collects energy while walking. The frequency is 0.67 Hz at 2 km/h and 2 Hz at 6 km/h, respectively.
[d]Maximum power generated (across 240 Ω optimum load) by the harvester while the swing-arm is at ±25 degrees rotational amplitude and 0.8 sec period (1.25 Hz).
[e]Under lab conditions with speed from 100 rpm to 800 rpm, where the max. output power at 200Ω load is 23.5mW. The distance between EM and GM is 20mm, same as that in [25].

Fig. 16. Test setup for WSN module power consumption measurement.

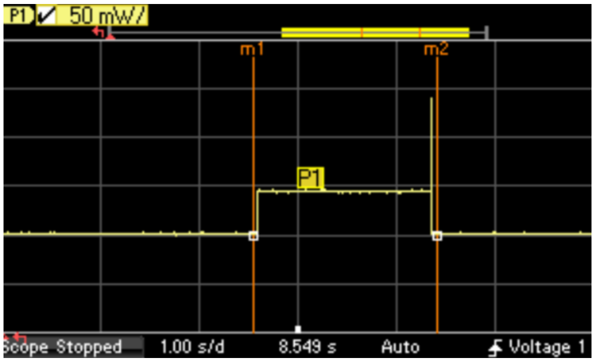

(a)

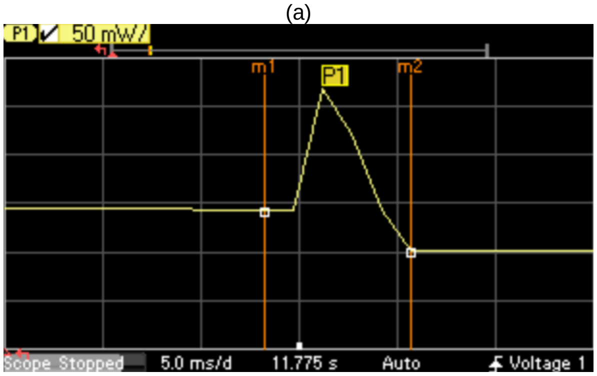

(b)

Fig. 17. Measured power consumption of the Zigbee sensor node (a) at active mode; (b) when transmitting data.

When the wireless wakes up from the PM2 sleep mode, it will enter active mode. During active mode, it will try to search for the coordinator and communicate with the coordinator. According to the measurement given above, this process consumes 73.8 mJ of energy in each attempt. If the sensor node attempts to connect too frequently, its energy storage will quickly deplete. Therefore, the wireless sensing node is programmed to make a maximum of five connection attempts after entering active mode every time. If the node fails to pair with the coordinator after five attempts, it is set to enter PM2 sleep mode and remain for five minutes to accrue enough energy in the storage.

VI. System Demonstration

In this work, fifteen wireless sensor nodes have been installed in a test bed specially constructed to mimic multiple rollers in operation. Due to the memory limitation of the CC2530 chip, a coordinator can only connect up to about sixty sensor nodes at a time. In practice, a coal mine conveyor has around four rollers per 0.75 meters. Given the communication range within tunnel conditions, deploying one coordinator per 75 meters of the conveyor would demand monitoring around 400 rollers in that stretch, exceeding the coordinator's maximum capacity of 60 sensor nodes as previously estimated. To solve this problem, the sensor node was programmed to actively exit the network and enter the sleep mode right after each data transmission. A clock is set to sequence wake and sleep cycles of the nodes. The wireless sensor nodes are active for approximately 2 seconds. The memory allocated to a specific sensor node within the coordinator is no longer occupied once that WSN node exits the network. If the coordinator's memory is exhausted, the request from a new wireless sensor node fails. The node enters sleep mode and awaits the next connection attempt for a predetermined amount of time. According to the requests from the potential users, the interval for collecting each roller's speed data can be up to 30 minutes or longer. As a result, for each 75-metre segment of the conveyor, there are 400 connections and data transactions in total for each 30 mins. A coordinator's maximum hosting capacity of is 54000 connections and transactions, which should be sufficient to host 400 sensor nodes. The proposed active withdrawal approach was implemented in the system demonstration and proved its effectiveness.

All the modules, including the energy harvester module, the power management unit, and the wireless sensing module, are integrated into a 68mm×52mm×25mm box. Fifteen wireless sensor node boxes are mounted to the test bed to monitor the rotational speeds of fifteen discs, which mimic rollers (each is equipped with one EM, as depicted inFig. 18). The discs rotate at various speeds ranging from 500 rpm to 1600 rpm. One minute after initiating the test bed, each sensor node begins transmitting the collected speed data to the coordinator. The speed data gathered by the coordinator is finally transmitted to the Alicloud platform via a robust 4G network connection. Following the activation of the testbed, a user interface comes alive on the display approximately one minute later, showcasing the real-time rotational velocities of all monitored discs. A picture of the interface having all fifteen discs' rotational speeds is shown inFig. 19. This visual representation encapsulates the dynamic performance of fifteen discs, each meticulously monitored by dedicated sensor nodes programmed to relay their data to the Zigbee coordinator on a minutely basis. Consequently, the interface refreshes with updated speed information for each disc every sixty seconds, enabling vigilant safety personnel to swiftly identify any anomalous behavior in the rollers Given the scope of our endeavor, we have yet to extend our testing to a comprehensive system equipped with four hundred sensor nodes. Nevertheless, the data transmission density observed in our demonstration—with fifteen sensor nodes actively sensing and transmitting data every minute—is analogous to that of a significantly larger network of four hundred nodes operating under similar conditions but with a considerably reduced frequency of data transmission. The successful demonstration of our system, albeit on a smaller scale, confidently projects its efficacy in monitoring an extensive number of rollers typically found in industrial conveyor systems, underscoring its potential for widespread application in the field.

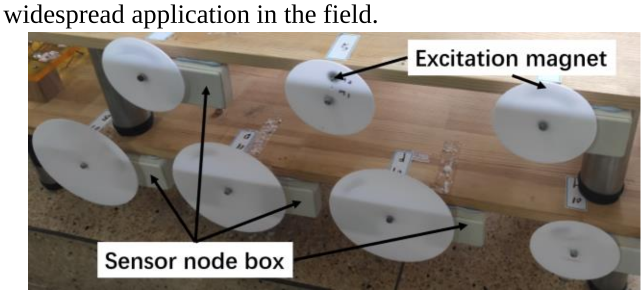

Fig. 18. Test bed for the wireless speed monitoring system.

This article has been accepted for publication in IEEE Sensors Journal. This is the author's version which has not been fully edited and content may change prior to final publication. Citation information: DOI 10.1109/JSEN.2024.3487757

Fig. 19. Alicloud based user interface showing the speed information.

VII. Conclusion

A novel real-time, self-powered wireless speed monitoring system has been successfully developed in this work for monitoring the rotational speed of rollers in belt conveyors. This innovative maintenance-free wireless sensing system comprises multiple wireless sensor nodes, a Zigbee coordinator, a 4G module, and an Ali Cloud Computing based visualization interface. Each compact wireless sensor node, housed within a 68mm×52mm×25mm plastic box, is equipped with an energy harvester, a power management unit, and a wireless sensing module. The energy harvester extracts energy from a rotating ring-shaped permanent magnet, which is driven by an external excitation magnet mounted on the roller. The energy harvester generates an output power of 23.5 mW at a high rotational speed of 800 rpm, thanks to the free-wheeling mechanism and the coil optimization. A comprehensive transient model has also been developed to accurately predict the harvester's performance even when the rotational status of the generating permanent magnet is random during operation. The power management unit ensures reliable rectification, storage, and regulation of the electrical power generated. The wireless sensing module collects speed information from rollers and transmits it to a base station connected to the cloud via a 4G telecommunication network. Ultimately, the real-time rotational speeds of all rollers are visualized using a custom-designed user interface. The effectiveness of the self-powered wireless roller speed monitoring system is successfully demonstrated in a test bed. Fifteen sensor nodes are programmed to sense and transmit data to the ZigBee coordinator every minute, ensuring that the displayed speeds for each roller are updated accordingly. Due to its wireless capabilities and kinetic energy harvesting technology, this system can be seamlessly integrated into existing conveyor belt systems without the need for any modifications. The system's battery-free design can significantly reduce maintenance costs and enhance its autonomy. In future research, while considering factors such as energy consumption, it may be beneficial to integrate additional sensors into the system to obtain more comprehensive and effective information. The system is yet to be demonstrated using a much larger number of sensor nodes, ideally in a real convey system.

References

[1] X. Guo, *et al.*, "Machine vision based damage detection for conveyor belt safety using Fusion knowledge distillation," *Alexandria Engineering Journal*, vol. 71, pp. 161-172, 2023/05/15/, 2023.
[2] S. K. Kommuri, *et al.*, "Sliding-Mode-Based Observer–Controller Structure for Fault-Resilient Control in DC Servomotors," in IEEE Transactions on Industrial Electronics, vol. 65, no. 1, pp. 918-929, Jan. 2018, doi: 10.1109/TIE.2017.2721883.
[3] Y. Gritli, *et al.*, "Advanced Diagnosis of Outer Cage Damage in Double-Squirrel-Cage Induction Motors Under Time-Varying Conditions Based on Wavelet Analysis," in IEEE Transactions on Industry Apps, vol. 50, no. 3, pp. 1791-1800, May-June 2014, doi: 10.1109/TIA.2013.2285958.
[4] G. Żak, A. Wyłomańska and R. Zimroz, "Local Damage Detection Method Based on Distribution Distances Applied to Time-Frequency Map of Vibration Signal," in IEEE Transactions on Industry Applications, vol. 54, no. 5, pp. 4091-4103, Sept.-Oct. 2018, doi: 10.1109/TIA.2018.2828787.
[5] X. Liu, *et al.*, "Experimental research on condition monitoring of belt conveyor idlers," *Measurement*, vol. 127, pp. 277-282, 2018.
[6] M. Fiset; D. Dussalt. "Laboratory simulation of the wear process of belt conveyor rollers," *Wear*, vol. 162, pp. 1012-1015, 1993.
[7] M. Andrejiova, A. Grincova, and D. Marasova, "Measurement and simulation of impact wear damage to industrial conveyor belts," *Wear*, vol. 368–369, pp. 400-407, 2016.
[8] X. P. Jiang, and G. Q. Cao, "Belt conveyor roller fault audio detection based on the wavelet neural network," in International Conference on Natural Computation(ICNC), Zhangjiajie, China, 2015, pp. 954-958.
[9] K. Su, *et al.*, "Hierarchical diagnosis of bearing faults using branch convolutional neural network considering noise interference and variable working conditions," *Knowledge-Based Sys*, vol. 230, pp. 107386, 2021.
[10] O. B. Akan, *et al.*, "Internet of Hybrid Energy Harvesting Things," *IEEE Internet of Things Journal*, vol. 5, no. 2, pp. 736-746, April 2018.
[11] Y. Ni, and L. Chen, "Research of energy saving control System of Mine belt conveyors," in 2021 International Conference on Intelligent Transportation, Big Data & Smart City (ICITBS), Xi'an, China, 2021, pp. 579-581.
[12] G. Lodewijks, "Strategies for Automated Maintenance of Belt Conveyor Systems," *Bulk Solids Handling: The International journal of Storing, Handling and Transporting Bulk*, no. 1, pp. 24, 2004.
[13] R. G. Ribeiro, *et al.*, "Unmanned Aerial Vehicle Location Routing Problem With Charging Stations for Belt Conveyor Inspection System in the Mining Industry," *IEEE Transactions on Intelligent Transportation Systems*, vol. 21, no. 10, pp. 4186-4195, 2020.
[14] E. Pievanelli, *et al.*, "Dynamic wireless sensor networks for real time safeguard of workers exposed to physical agents in constructions sites," in IEEE Topical Conference on Wireless Sensors & Sensor Networks, Austin, TX, USA, 2013, pp. 55-57.
[15] A. Chunawale, and S. Sirsikar, "Minimization of average energy consumption to prolong lifetime of Wireless Sensor Network," in IEEE Global Conference on Wireless Computing & Networking(GCWCN), Lonavala, India, 2014, pp. 244-248.
[16] O. B. Akan, *et al.*, "Internet of Hybrid Energy Harvesting Things," *IEEE Internet of Things Journal*, vol. 5, no. 2, pp. 736-746, April 2018.
[17] H. Fu, *et al.*, "Rotational energy harvesting for self-powered sensing," *Joule*, vol. 5, no. 5, pp. 1074-1118, 2021.
[18] Z. Sui, *et al.*, "Piezoelectric Based Smart Tire for Vehicle Speed and Load Detection and Energy Harvesting," in 2021 IEEE International Conference on Flexible and Printable Sensors and Systems (FLEPS), Manchester, United Kingdom, 2021, pp. 1-4.
[19] H. Aliniagerdroudbari, *et al.*, "A piezoelectric sandwich structure for harvesting energy from tire strain to power up intelligent tire sensors," in 2019 IEEE Power and Energy Conference at Illinois (PECI), Champaign, IL, USA, 2019, pp. 1-7.
[20] J. Kan, *et al.*, "Energy harvesting from wind by an axially retractable bracket-shaped piezoelectric vibrator excited by magnetic force," *Energy*, vol. 240, 2022.
[21] J. Zhang, *et al.*, "A rotational piezoelectric energy harvester for efficient wind energy harvesting," *Sensors and Actuators A: Physical*, vol. 262, pp. 123-129, 2017.
[22] D. Dinulovic, *et al.*, "Portable rotational electromagnetic energy harvester with a maximum energy tracking power management system," in International Symposium on Power Electronics(Ee), Novi Sad, Serbia, 2017, pp. 1-6.

[23] Y.Y. Feng, *et al.*, “An Electromagnetic Energy Harvester for Extracting Rotational Energy,” in 2018 IEEE 7th Global Conference on Consumer Electronics (GCCE), Nara, Japan, 2018, pp. 708-709.
[24] K. I. Lee, *et al.*, “Energy harvesting by rotation of wheel for tire monitoring system,” in SENSORS, 2012 IEEE, Taipei, Taiwan, 2012, pp. 1-4.
[25] G. Miao, *et al.*, “A low-frequency rotational electromagnetic energy harvester using a magnetic plucking mechanism,” *Applied Energy,* vol. 305, pp. 117838, 2022.
[26] D. Xiaoyi, *et al.*, “A hybrid energy harvesting system for self-powered applications in shared bicycles,” *Sustainable Energy Technologies and Assessments,* vol. 51, pp. 101891, 2022.
[27] J. Lin, *et al.*, “A rotational wearable energy harvester for human motion,” in 2017 IEEE 17th International Conference on Nanotechnology (IEEE-NANO), Pittsburgh,PA, USA, 2017, pp. 22-25.
[28] M. A. Halim, *et al.*, “Electromagnetic energy harvesting from swing-arm motion using rotational eccentric mass structure,” in International Conference on Solid-state Sensors(TRANSDUCERS), Kaohsiung, Taiwan, 2017, pp. 1863-1866.
[29] Y. J. Wang, *et al.*, “System Design of a Weighted-Pendulum-Type Electromagnetic Generator for Harvesting Energy From a Rotating Wheel,” *IEEE/ASME Transactions on Mechatronics,* vol. 18, no. 2, pp. 754-763, 2013.
[30] S. Motoyama, *et al.*, “The Contactless Permanent Magnet Energy Harvester using Gyration from Roller Conveyor,” in 2019 8th International Conference on Renewable Energy Research and Applications (ICRERA), Brasov, Romania, 2019, pp. 987-990.

Shiheng Zhou received the B. S. degree from the Wenzhou University in 2016, and the M.Eng.Sc. degree from Hanzhou Electronic Science and Technology University in 2023 majored in electronic science and technology. He is currently working as a R&D engineer. His research interests include electromagnetic energy harvesting, power management, and low power wireless sensing technology.

Tingcong Ye received the BA degree in electrical information engineering from Guilin University of Electronic and Technology in China in 2007. He received his MEngSc and PhD degree from University College Cork in Ireland, in 2009 and 2016, respectively. He joined the Hangzhou Dianzi University as a lecturer in 2017. His research interests include design and optimization of wireless localization systems, low power embedded systems and energy harvesting devices.

Lei Liu received the B. S. and M. S. degrees from the Hefei University of Technology, in 2004 and 2007, respectively, and the D. Eng. Degree from Zhejiang University, Hangzhou, China, in 2012, all in electrical engineering. He has been a lecturer with the school of electronics and information engineering in Hangzhou Dianzi University since 2020. His research interests include inverse problems in electromagnetics.

Zhengmin Zhang received the B. S. degree from the Shandong University in 2010, and the PhD degree from the University of Chinese Academy of Sciences in 2015, majored in microelectronics and solid electronics. He has been a lecturer with the school of electronics and information engineering, Hangzhou Dianzi University since 2020. His research interests include analog integrated circuit design, CMOS image sensor, power management IC, and ultra low power consumption power management for energy harvesting system.

Mike Hayes received the M.Eng.Sc. degree from the University College Cork, Cork, Ireland, in 1987. In 2008, he brought over 20 years electronics technical & managerial experience to Tyndall as industry-led Program Manager for ICT enabled technologies for energy efficiency applications. This includes development of wireless sensor network platforms, energy harvesting systems, and conditional monitoring solutions & power electronics for EU, Irish, & industry partners. He is a work package leader on several EU projects (MOSYCOUSIS ARTEMIS ME3Gas, GreenCom) and coordinates IERC project ROWBUST (www.ierc.ie) developing energy harvesting, quality of service, and autocommissioning and return on investment models for wireless sensors.

Ningning Wang received the B.S.E.E. and M.Sc. degrees in electrical engineering from Xi’an Jiaotong University, Xi’an, China, in 1995 and 1998, respectively, and the Ph.D. degree from University College Cork, Cork, Ireland, in 2005. He joined the Tyndall National Institute, Cork, as a Postdoctoral Researcher in 2005 and was appointed as a permanent Staff Researcher in early 2008. He joined Hangzhou Dianzi University in 2018 as a professor. He has extensive research experience in design, modeling, and fabrication of integrated magnetics for power conversion and energy harvesting for wireless sensor network applications. He has participated and managed a number of research projects supported by national and provincial funding agencies, EU research funds, and industrial partners in the domains of integrated magnetics for power conversion applications, and energy harvesting and power management for wireless sensor networks.